Journal of Materials Chemistry A

Electrocatalysis of layered group 5 metallic transition metal dichalcogenides (MX2, M=V, Nb, Ta; X= S, Se, Te)

Journal:	*Journal of Materials Chemistry A*
Manuscript ID	TA-ART-06-2016-005110.R1
Article Type:	Paper
Date Submitted by the Author:	03-Aug-2016
Complete List of Authors:	Chia, Xinyi; Nanyang Technological University, Chemistry and Biological Chemistry Ambrosi, Adriano; Nanyang Technological University, Chemistry and Biological Chemistry Lazar, Petr; Palacky University Olomouc, Department of Physical Chemistry Sofer, Zdenek; Institute of Chemical Technology, Prague, Department of Inorganic Chemistry Pumera, Martin; Nanyang Technological University, Chemistry and Biological Chemistry

Journal Name

ARTICLE

Electrocatalysis of layered Group 5 metallic transition metal dichalcogenides (MX_2, M=V, Nb, Ta; X= S, Se, Te)

Received 00th January 20xx,
Accepted 00th January 20xx

DOI: 10.1039/x0xx00000x

www.rsc.org/

Xinyi Chia,[a] Adriano Ambrosi,[a] Petr Lazar,[bc] Zdenek Sofer[d] and Martin Pumera[a]*

The revelation of MoS_2 as an efficient electrocatalyst for hydrogen evolution reaction (HER) has ratcheted up interest in other transition metal dichalcogenides (TMDs). To date, extensive studies have been inclined towards semiconducting Group 6 TMDs while research into metallic Group 5 TMDs is comparatively limited. Past computational screening of Group 5 TMDs showed propitious Gibbs free energy of the adsorbed hydrogen (ΔG_H) for HER, especially for VS_2, which prompted us to experimentally explore their HER efficiency. In addition to the HER electrocatalytic performance, we examine the inherent electrochemistry and the charge-transfer property of the entire set of Group 5 TMDs in the bulk form: VS_2, VSe_2, VTe_2, NbS_2, $NbSe_2$, $NbTe_2$, TaS_2, $TaSe_2$ and $TaTe_2$. We demonstrate that the nine Group 5 TMDs show distinctive inherent electroactivities arising from their intrinsic electrochemical processes or surface oxides. TaS_2 possesses fastest heterogeneous electron transfer (HET) rate at 3.4×10^{-3} cm s^{-1} amongst the Group 5 TMDs and may be ideal for electrochemical sensing. Chalcogen-dependence is evident in the electrochemical charge-transfer ability of the Group 5 TMDs whereby tellurides show slower HET rates than sulfides and selenides. We identify VTe_2 as the best-performing material for HER contrary to the widely predicted VS_2. VTe_2 manifests lowest HER overpotential at 0.5 V *vs*. RHE and Tafel slope of 55 mV/dec. Interestingly, the HER performance of vanadium dichalcogenides and Group 5 tellurides show chalcogen- and transition metal- dependence respectively. Reasons behind their HER performance have also been proposed from our theoretical studies founded on thermodynamics and kinetics. Broadly, the HER performances of bulk Group 5 TMDs are less outstanding than expected despite being true metals. This fundamental study provides fresh insights into the electrochemical and electrocatalytic characteristics of metallic Group 5 TMDs that will be indispensable for the development of TMDs in future applications.

Introduction

Research into layered transition metal dichalcogenides (TMDs) is gradually gaining ground within the scientific community. Taking on a general formula of MX_2, a TMD consists of a transition metal from groups 4-10 and a chalcogen (S, Se, Te), respectively denoted as M and X MoS_2, the archetypal TMD belonging to Group 6, has basked in the glory of its achievements to date, with a long list of promising uses in catalysis,[1-6] sensing,[7] energy storage and conversion.[8-10] The success of MoS_2 revved up interest in other classes of TMDs beyond the semiconducting Group 6. Most notably, the Group 5 TMDs (where M= V, Nb, Ta and X= S, Se and Te) which are of metallic conductivity have stolen the limelight. . This class of materials is prized for their low-dimensional crystal structure and exhibits interesting electronic properties such as superconductivity, charge density waves and Mott transition.[11, 12] However, unlike MoS_2, the electrochemical and electrocatalytic properties of the Group 5 TMDs have not been well-established at the moment.

At present, assiduous studies centering on the layered TMDs seek to provide an efficient electrocatalyst for hydrogen evolution reaction (HER). Hydrogen gas is raved as a "clean" energy candidate. Hydrogen production involves the electrolysis of water either by electrical or solar means and emits environmental-friendly oxygen as its by-product.[13] However, the process is thermodynamically unfavourable and requires an efficient electrocatalyst to facilitate the reaction. Currently, platinum (Pt) has been identified as the most efficient electrocatalyst. The drawback of Pt lies in its low natural abundance which inflates the cost of hydrogen production. Hence, the fervent pursuit to explore efficient and earth-abundant alternatives in a bid to lower production cost. MoS_2 is one of the rising stars in the quest for alternatives due

[a] *Division of Chemistry and Biological Chemistry, School of Physical and Mathematical Sciences, Nanyang Technological University, Singapore 63737, Singapore. Email: pumera@ntu.edu.sg*
[b] *Department of Physical Chemistry, Palacký University Olomouc, tř. 17. Listopadu 1192/12, 771 46 Olomouc, Czech Republic..*
[c] *Department of Physical Chemistry, Regional Centre of Advanced Technologies and Materials, tř. 17. Listopadu 1192/12, 771 46 Olomouc, Czech Republic.*
[d] *Department of Inorganic Chemistry, University of Chemistry and Technology Prague, Technicka 5, 166 28, Prague 6, Czech Republic.*

† Electronic Supplementary Information (ESI) available: Energy-dispersive X-ray spectra; scanning electron micrographs; energy-dispersive X-ray maps; high resolution and wide scan X-ray photoelectron spectra; tabulated chalcogen-to-metal ratios; cyclic voltammograms for Group 5 oxides; tabulated heterogeneous electron transfer rate constants; linear sweep voltammograms; tabulated exchange current densities; electronic band structures. See DOI: 10.1039/x0xx00000x

to its competent HER performance[3, 4] and its high natural abundance. The edges of MoS_2 are found to be the catalytic sites for HER.[14, 15] Other layered TMDs, mainly members from Group 6, have also been studied for their HER efficiency.[16-18] Based on the recent spate of density functional theory calculations[19, 20] performed on Group 5 TMDs, they are postulated to be favorable electrocatalysts. Having close to thermoneutral Gibbs free energy of the adsorbed hydrogen (ΔG_H), the basal planes of the VS_2, NbS_2 and TaS_2 are considered supplementary HER active sites to their edges.[20] The theoretical finding is verified insofar as the stellar HER efficiency of VS_2 synthesized by chemical vapour deposition that was recently reported by Yuan *et al*.[21]

There is strong dependence of the electronic structure of the TMDs on the coordination of the transition metal centre and its d-electron count which confers Group 6 to be semiconducting while Group 5 are true metals.[22] Lukowski *et al.* demonstrated that the HER efficiency of semiconducting Group 6 TMDs, specifically for MoS_2 and WS_2, improved dramatically after undergoing a transition from semiconducting 2H- to metallic 1T- phase *via* chemical exfoliation.[23] The enhanced HER performance of metallic 1T-MoS_2 and 1T-WS_2, compared to their respective semiconducting 2H-phases, have been attributed to the faster electrode kinetics and proliferation of the catalytic sites which includes the basal planes in the metallic 1T polymorph. Given that Group 5 TMDs are also largely metallic by nature regardless 1T or 2H, they may rival or even surpass the HER performance exhibited by the semiconducting Group 6 TMDs.

Although the metallic nature and favourable ΔG_H of the Group 5 TMDs are touted to be advantageous for HER, this has not been experimentally substantiated yet. Herein, we experimentally demonstrate the HER efficiency for the complete set of Group 5 TMDs in the bulk form and determine the best electrocatalyst among them. The HER electrocatalytic trends of the Group 5 TMDs are also discussed along with our theoretical studies. Besides their electrocatalytic properties, we also investigate the electrochemistry of the Group 5 TMDs and evaluate their electrochemical charge-transfer property. Systematic characterisation of the materials *via* scanning electron microscopy (SEM), energy-dispersive X-ray spectroscopy (EDS) and X-ray photoelectron spectroscopy (XPS) are also performed. The nine Group 5 TMDs that are explored in this paper include VS_2, VSe_2, VTe_2, NbS_2, $NbSe_2$, $NbTe_2$, TaS_2, $TaSe_2$ and $TaTe_2$.

Results and Discussion

Characterisation

Prior to any electroanalysis of the Group 5 transition metal dichalcogenides (TMDs), we perform material characterization using scanning electron microscopy (SEM), energy-dispersive X-ray spectroscopy (EDS) and X-ray photoelectron spectroscopy (XPS).

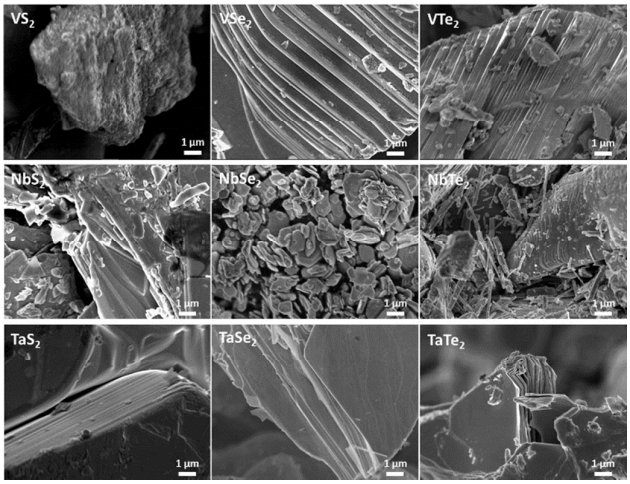

Fig. 1 Scanning electron micrographs of the various Group 5 TMDs at a magnification of 10 000 ×. Scale bars represent 1 µm.

We examine the surface morphologies of the Group 5 TMDs by SEM. It is deduced that all samples demonstrate structural features typical of bulk materials. VS_2 appears as predominantly large pieces, a stark contrast to VSe_2 and VTe_2 with layered appearance. Between VSe_2 and VTe_2, VSe_2 sheets are accordion-like and exhibit wider interlayer separation. Niobium materials; NbS_2, $NbSe_2$ and $NbTe_2$, manifest in irregular shapes. Large pieces with structures vaguely resembling thick layers and uneven ridges are apparent for NbS_2 and $NbTe_2$, respectively while $NbSe_2$ exist in smaller pieces. All tantalum materials; TaS_2, $TaSe_2$ and $TaTe_2$, are found to be layers in close stacking with definite edges and basal planes. The calculated chalcogen-to-metal ratios on the basis of EDS for all Group 5 TMDs fall within the range of 1.5 and 2.1, approximating the projected stoichiometric ratio of 2.0 (as recorded in Table S1 and the corresponding spectra and maps are presented in Fig. S1 and S2 of ESI†).

Using XPS, we analyse the surface elemental composition and bonding information of the Group 5 TMDs up to a maximum depth of 10 nm. This will be useful towards understanding their electrochemistry which involves electron transfer processes on the surface of the material. The high-resolution spectra of V 2p, Nb 3d and Ta 4f peaks are illustrated in Fig. 2 and their estimated distributions of the numerous oxidation states are presented in Tables S3.1-S3.3 (in ESI†).

Based on XPS deconvolution of the Group 5 transition metal into various oxidation states, all Group 5 TMDs, except NbS_2, adopt +4 (denoted as the red line) as the principal state, concurring with the expected oxidation state in a dichalcogenide. Due to the proximity of the O 1s and V 2p signals, O 1s occurring at *ca.* 530 eV is also included to yield a relatively level baseline and a better XPS fitting for V 2p.[24] Evident in VS_2, VSe_2, and VTe_2, the fitted peaks for V 2p exhibit V^{4+} as the dominant species with significant contribution originating from the V $2p_{3/2}$ and V $2p_{1/2}$ signals at *ca.* 516.0 eV and 523.4 eV. These signals lie close to the reported literature values of 515.6 eV and 523.0 eV.[25] Similarly, the tantalum

dichalcogenides; TaS_2, $TaSe_2$ and $TaTe_2$ also show the primary Ta 4f signal is attributed to the Ta^{4+} species as manifested in Ta $4f_{7/2}$ and Ta $4f_{5/2}$ binding energies of *ca.* 26.3 eV and 28.2 eV, in close agreement with an early study by McGuire *et al.*[26] While the main Nb $3d_{5/2}$ and Nb $3d_{3/2}$ binding energies in $NbSe_2$ and $NbTe_2$ at *ca.* 206.2 eV and 209.0 eV are characteristic of the Nb^{4+} species,[26, 27] the bulk of Nb 3d signals in NbS_2 are attributed to the presence of Nb^{2+} and Nb^{5+}. Prominent peaks of Nb $3d_{5/2}$ binding energies in NbS_2 at *ca.* 203.7 eV and 207.7 eV correspond to the respective Nb(II) and Nb(V) states.[27]

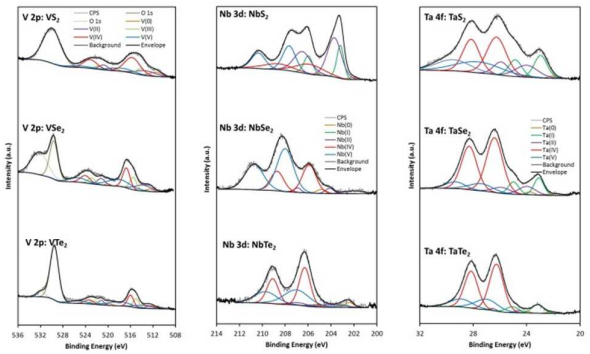

Fig. 2 High resolution X-ray photoelectron spectra of V 2p, Nb 3d and Ta 4f regions of the Group 5 TMDs. The deconvoluted peaks correspond to the numerous oxidation states of V, Nb and Ta.

Apart from the anticipated +4 oxidation state of the Group 5 transition metal, it is noteworthy that a substantial contribution from the +5 oxidation state is also detected in all Group 5 TMDs. Given the considerable oxygen content observed in the survey XPS scans for all materials (Table S5 in ESI†), transition metal oxides occurring in the +5 oxidation state may be present. In vanadium dichalcogenides, the presence of V^{5+} species is indicated by the V $2p_{3/2}$ signal at *ca.* 517.8 eV which nears the V $2p_{3/2}$ binding energy of V_2O_5.[28, 29] As the pentavalent state is found to be most stable oxidation state for niobium and tantalum,[30] its occurrence is no wonder. The peaks at *ca.* 207.7 eV and 210.4 eV, most noticeably in NbS_2 and $NbSe_2$, coincide with the Nb $3d_{5/2}$ and Nb $3d_{3/2}$ binding energies of Nb_2O_5.[31] The Ta $4f_{7/2}$ and $4f_{5/2}$ binding energies of Ta^{5+} species at *ca.* 27.6 eV and 29.5 eV in TaS_2, $TaSe_2$ and $TaTe_2$ lies in good agreement with the literature values reported for Ta_2O_5.[26, 32]

In addition to the main XPS signal in tantalum dichalcogenides belonging to the Ta(IV) state, a distinctive shoulder signal at *ca.* 22.1 eV exists across TaS_2, $TaSe_2$ and $TaTe_2$. This signal is attributed to the Ta $4f_{7/2}$ binding energy of Ta(I) state[33] which may be speculated to be in the form of Ta_2O due to the high oxygen content detected (Table S5 in ESI†).

XPS deconvolution of the respective chalcogen of the Group 5 TMDs is shown in Fig. S4 (in ESI†). In theory, the oxidation state of S, Se and Te chalcogen in all Group 5 TMDs is -2. Analysis of S 2p core level indicates the existence of S^{2-} species in VS_2, NbS_2 and TaS_2, and the peaks at *ca.* 160.8 eV and 162.0 eV are respectively indexed to S $2p_{3/2}$ and S $2p_{1/2}$, appearing as a merged signal in VS_2 and as distinct signals in NbS_2 and TaS_2. A sulfate signal is also visible at a binding energy of 168.0 eV in VS_2, suggesting trace presence of SO_4^{2-} in VS_2.[34] Deconvolution of Se 3d core level reveals that Se(0) and Se(-II) species exist in VSe_2, $NbSe_2$ and $TaSe_2$, wherein the observed peak at *ca.* 55.2 eV is attributed to Se(0) while Se^{2-} accounts for the other peak at *ca.* 53.5 eV.[35] Clearly, Group 5 sulfides and selenides possess a reasonable portion existing in the oxidation state of +2, concurring with the expected. Conversely, fitted peaks for Te 3d in Group 5 tellurides show that the majority is attributed to the Te(IV) species, most likely occurring as TeO_2, with significant contribution stemming from its characteristic doublets at *ca.* 575.3 eV and 585.6 eV corresponding to Te $3d_{5/2}$ and $3d_{3/2}$ binding energies.[36, 37] Besides TeO_2, TeO_3 was also suggested to be present on the surface of the Group 5 TMDs as noted from the contribution of the Te $3d_{5/2}$ binding energy at *ca.* 576.3 eV. The anticipated Te^{2-} was detected, in visibly lower amounts relative to TeO_2, with its distinctive paired peaks of Te $3d_{5/2}$ and $3d_{3/2}$ signals at *ca.* 571.6 and 582 eV.[37, 38] It can be rationalized that substantial amount of Te oxides formed, including TeO_2 and TeO_3, because the tellurides are more liable towards surface oxidation than sulfides or selenides.[39]

Interestingly, the calculated chalcogen-to-metal ratio of the Group 5 TMDs based on XPS analysis (Table S3.1-S3.3, in ESI†) reveals that the surface composition of tellurides are chalcogen-enriched whereas the selenides and sulfides are chalcogen-deficient. VTe_2 has a XPS chalcogen-to-metal ratio of 2.0, coinciding with the projected ratio. Other tellurides, $NbTe_2$ and $TaTe_2$, exhibit chalcogen-enriched surfaces with ratios beyond 2.0; at 3.0 and 2.6 respectively. On the contrary to the tellurides, both sulfides and selenides demonstrate a ratio lower than the expected 2.0. Specifically, VS_2, NbS_2 and TaS_2 show ratios at 1.1, 1.6 and 1.1 respectively. The selenides; VSe_2, $NbSe_2$ and $TaSe_2$, have ratios at *ca.* 1.0. With the exception of VTe_2, we notice that the chalcogen-to-metal ratio for all the Group 5 TMDs provided by XPS analysis deviate considerably from 2.0. Conversely, the ratio derived from EDS analysis lies close to the ideal 2.0 (Table S2, in ESI†). This disparity between the chalcogen-to-metal ratio provided by EDS and XPS analyses likely arises from the differences in surface composition and the bulk composition of the Group 5 TMDs, with possible passivation by surface oxides.

Inherent electrochemistry

Presently, there has been inadequate research directed towards exploring the inherent electrochemistry of VS_2, VSe_2, VTe_2, NbS_2, $NbSe_2$, $NbTe_2$, TaS_2, $TaSe_2$ and $TaTe_2$. Inherent electrochemistry has been understood to be the characteristic redox reaction of the material when an electrochemical potential is applied.[40] Due to the different intrinsic components of the Group 5 TMDs, in terms of the transition metal or chalcogen type, the various Group 5 TMD materials are expectedly dissimilar in electrochemical behavior. Determining the inherent electrochemistry of Group 5 TMDs is crucial when designing electrochemical applications; in

particular in electrochemical sensing, because the innate signals may limit its operational potential window.[41] It is also of interest to note the effect of transition metal or chalcogen type on the inherent electrochemistry. With these ends in view, we studied the inherent electrochemistry of all Group 5 TMDs and their voltammograms are presented in Fig. 3. Anodic and cathodic scan directions were performed in three consecutive scans to provide electrochemical information and establish the nature of the redox processes occurring on the surface of Group 5 TMDs.

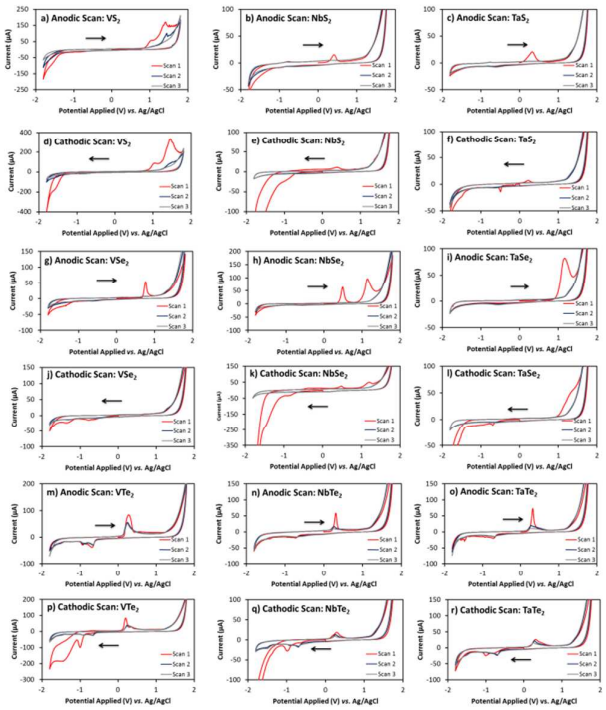

Fig. 3 Cyclic voltammograms recording the inherent electrochemistry of the various Group 5 TMDs; namely, Group 5 sulfides during the anodic (a-c) and cathodic (d-f) scans, Group 5 selenides during the anodic (g-i) and cathodic (j-l) scans and the Group 5 tellurides during the anodic (m-o) and cathodic (p-r) scans. Conditions: background electrolyte, PBS (50 mM), pH 7.0; scan rate, 100 mV s^{-1}; scans begin at 0.0 V *vs.* Ag/AgCl. The arrows denote initial scan direction.

Due to the extensive oxide contribution on the surface of most Group 5 TMDs, cyclic voltammetry of the more predominant Group 5 oxides has been conducted including V_2O_5, Nb_2O_5 and Ta_2O_5 (recorded in Fig. S5, in ESI†). Comparing the redox signals of the Group 5 TMDs with that of the respective oxides, we notice several signals that are coincident. These signals may shed light on the electrochemical process occurring on the material. Among all vanadium dichalcogenides, the cathodic scan of VSe_2 exhibits two reduction signals at *ca*. -0.8 V and -1.4 V *vs.* Ag/AgCl (Fig. 3j) matching the characteristic cathodic peaks in V_2O_5 (Fig. S5b in ESI†). Performing cyclic voltammetric scans on compounds of V(V) oxidation state; V_2O_5, $NaVO_3$ and Na_3VO_4, Ryan *et al.* proposed that the two reduction peaks observed at 1.4 V and 0.5 V *vs.* Al/$AlCl_3$ in V_2O_5 originate from two different kinds of V(V) species whereby each undergoes a single electron reduction process into the V(IV) species.[42] Similarly, we may infer that the inherent electrochemistry of VSe_2 involves two distinct types of V(V) species reducing to V(IV) species. Both VS_2 and VTe_2 show a cathodic signal at *ca.* -1.5 V *vs.* Ag/AgCl (Fig. 3d, 3p) that likely involves the reduction of a single type of V(V) species into V(IV) species. There are few similarities between the inherent electrochemistry of niobium dichalcogenides and Nb_2O_5 except for $NbTe_2$. Consistent with the cathodic signal noted in Nb_2O_5 (Fig. S5c, S5d in ESI†), $NbTe_2$ observes a reduction peak at *ca.* -0.6 V *vs.* Ag/AgCl (Fig. 3n, 3q) that aligns with a previous study which reported on the one-electron reduction of Nb(V) to Nb(IV) species occurring at -0.11 V *vs.* Ni/Ni^{2+}.[43] Across tantalum dichalcogenides, the inherent electrochemistry of Ta_2O_5 is apparent. TaS_2 exhibits a cathodic peak *ca.* -0.5 V *vs.* Ag/AgCl (Fig. 3f), coinciding with the standard reduction potential of Ta_2O_5 as formerly reported in literature to be -0.75 V *vs.* SHE.[44] The cyclic voltammograms obtained for Ta_2O_5 depicts a cathodic peak *ca.* -0.6 V *vs.* Ag/AgCl which is also relatively close to the reported values. The cathodic sweep for $TaSe_2$ and the anodic sweep for $TaTe_2$, each possess a reduction signal at *ca.* -0.6 V *vs.* Ag/AgCl corresponding to the reduction of Ta_2O_5 as experimentally shown. Ta oxide formation occurs at approximately 0.3 V *vs.* SCE. In particular, the anodic scans of TaS_2 and $TaTe_2$ showcases an oxidation peak at *ca.* 0.3 V *vs.* Ag/AgCl could possibly be due to Ta oxide formation.[45]

Scrutinizing further, we observe that that the inherent electrochemistry of niobium dichalcogenides forge close resemblance to that of the tantalum dichalcogenides. Beginning with their sulfides, the anodic scans of NbS_2 and TaS_2 reveal a moderate peak at *ca.* 0.4 V *vs.* Ag/AgCl. This signal may correspond to the oxidation of respective transition metal in oxidation state +4 into +5. Literature has also shown that the oxidation of Nb(VI) to Nb(V) occurs at -0.4 V *vs.* Al/Al^{3+},[46] existing close to our experimental signal when converted to *vs.* Ag/AgCl. While $NbSe_2$ has two distinct anodic signals at *ca.* 0.5 V and 1.2 V *vs.* Ag/AgCl, $TaSe_2$ shows only a single anodic signal. Both $NbSe_2$ and $TaSe_2$ share the conspicuous signal at *ca.* 1.2 V *vs.* Ag/AgCl of similar current intensity *ca.* 90 μA. For $TaSe_2$, the passivation of the surface with Ta_2O_5 is plausible and found to occur at potentials between 1.2 V and 2.0 V *vs.* Ag/AgCl.[47] The anodic scans of $NbTe_2$ and $TaTe_2$ are almost identical. During the anodic scan, a well-defined oxidation peak emerges at *ca.* 0.3 V *vs.* Ag/AgCl followed by an inconspicuous reduction signal at *ca.* -0.7 V *vs.* Ag/AgCl. Intriguingly, with subsequent scans in $NbTe_2$ and $TaTe_2$, the oxidation peak at *ca.* 0.3 V *vs.* Ag/AgCl also declines by the same magnitude. Despite the similarities between the anodic scans, their corresponding cathodic scans showcase distinguishing features. Cathodic scans of NbS_2 and $NbSe_2$ display a shoulder signal at *ca.* -0.8 V *vs.* Ag/AgCl that alludes to the reduction of Nb(V) to Nb(III) species *via* a two-electron process.[48, 49] In TaS_2 and $TaSe_2$, the Ta_2O_5 reduction signal is visible in the cathodic scans.

The inherent electrochemistry of tellurium is clearly exemplified in VTe_2, $NbTe_2$ and $TaTe_2$, given their unusually similar voltammetric profiles. All tellurides (VTe_2, $NbTe_2$ and

$TaTe_2$) demonstrate anodic signals at *ca.* 0.3 V *vs.* Ag/AgCl in both anodic and cathodic sweeps which coincide with the oxidative stripping of Te.[50] Moreover, VTe_2, $NbTe_2$ and $TaTe_2$, each has a reduction signal at *ca.* -1.0 V *vs.* Ag/AgCl during their cathodic scan. This reduction signal can be ascribed to Te reduction to soluble Te^{2-} species.[51] In subsequent cathodic scans, it is noted that this particular signal disappears and another reduction signal materializes at *ca.* -0.7 V *vs.* Ag/AgCl. However, *ca.* -0.7 V *vs.* Ag/AgCl is also present in the anodic scans. Hence, the oxidative feature at *ca*. 0.3 V *vs.* Ag/AgCl is a prerequisite to the subsequent signal at *ca*. -0.7 V *vs*. Ag/AgCl in the cathodic scan. Akin to the reduction signal at *ca.* -1.0 V *vs*. Ag/AgCl, this subsequent signal stems from the cathodic stripping of Te,[50] except occurring at a lower potential.

The inherent electrochemistry of the vanadium dichalcogenides has inadvertently unveiled that the oxidation potential increases from VTe_2 <VSe_2 <VS_2 in the order of the respective chalcogen within the group. In brief, VTe_2 exhibits an anodic signal at *ca*. 0.3 V *vs.* Ag/AgCl; and VSe_2, at *ca.* 0.8 V *vs.* Ag/AgCl; while VS_2 has two signals, at *ca*. 1.0 V and 1.4 V *vs*. Ag/AgCl. These signals result from the electrochemistry of the corresponding chalcogens on the basis of Pourbaix diagrams. At *ca.* 0.4 V *vs.* Ag/AgCl, the Te chalcogen in VTe_2 existing in oxidation state of -2 may oxidize to form species in states of +4 and +6, such as TeO_2, $HTeO_3^-$ and $HTeO_4^-$.[52] For VSe_2, the Se chalcogen undergoes an oxidation from -2 to +4 or +6 states at *ca.* 0.8 V *vs.* Ag/AgCl to yield $HSeO_3^-$, SeO_3^{2-} or SeO_4^{2-}.[53] At highly anodic potentials beyond ca. 1.0 V vs. Ag/AgCl, the S chalcogen in VS_2 may oxidize into thermodynamically stable species like HSO_4^- and SO_4^{2-}.[54] Furthermore, the phenomenon of escalating oxidation potentials from VTe_2 <VSe_2 <VS_2 concurs with the susceptibility of the chalcogen type towards oxidation. The tendency for oxidation amplifies down the chalcogen group: S <Se <Te, in which the tellurides succumb to surface corrosion most readily.[39]

Judging from subsequent scans, we determine, the nature of most electrochemical processes associated with the characteristic oxidation and reductions of the Group 5 TMDs, to be largely chemically irreversible. As observed in Fig. 3, majority of the unique redox signals in the initial scans become diminished in current intensity or vanished completely in subsequent scans. Anomalous to the general trend, the tellurides maintained current intensities of their reduction signal at *ca.* -0.7 V *vs.* Ag/AgCl and oxidation peak at *ca.* 0.3 V *vs.* Ag/AgCl in the following anodic and cathodic cycles. Such features are attributed to the reversible nature of Te(-II) oxidation as determined by Lingane *et al.*[55]

All the Group 5 TMDs studied exhibit electrochemistry that may be intrinsic to their surface oxides in addition to their respective metal or chalcogen components. In particular, the inherent electrochemistry of the tellurium chalcogen is most accentuated in the voltammograms of all Group 5 tellurides.

Heterogeneous electron transfer (HET) property

The heterogeneous electron transfer (HET) rate of an electrode material is a useful performance indicator towards evaluating the suitability of that material in electrochemical applications. An intrinsically fast HET rate lowers the overpotential required for an electrochemical reaction, and hence deemed a desirable attribute of a prospective electrode material. The classical Nicholson approach correlates the peak-to-peak separation (ΔE) with the observed HET rate constant (k^0_{obs}), whereby smaller ΔE corresponds to faster HET rates. The surface-sensitive nature[56] of $[Fe(CN)_6]^{3-/4-}$ redox probe will be beneficial when examining the HET rates of the Group 5 TMDs. The voltammetric profiles of $[Fe(CN)_6]^{3-/4-}$ on the Group 5 TMDs are depicted in Fig. 4 (with a summary of all ΔE summarized in a histogram in Fig. S6 in ESI†) and their k^0_{obs} are recorded in Table S6 (in ESI†). It is also important to note that the depicted voltammograms and computed k^0_{obs} values were extracted from the subsequent cycles. Due to strong interference by the inherent electrochemical signals of several Group 5 TMDs in the initial scan cycles within the potential window of -0.4 and 0.7 V *vs.* Ag/AgCl, the observations of $[Fe(CN)_6]^{3-/4-}$ redox signals may be unreliable in the initial cycles and hence, data from subsequent scans were used instead.

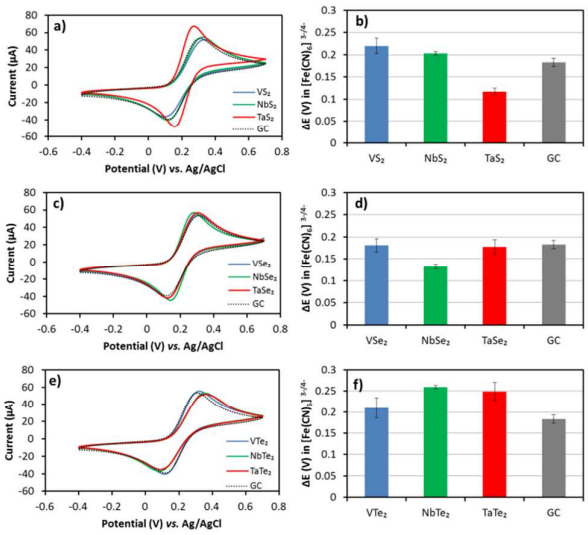

Fig. 4 Cyclic voltammograms of 5 mM $[Fe(CN)_6]^{3-/4-}$ on (a) Group 5 sulfides, (c) Group 5 selenides and (e) Group 5 tellurides. Peak separations for $[Fe(CN)_6]^{3-/4-}$ redox probe on the surfaces of (b) Group 5 sulfides, (d) Group 5 selenides and (f) Group 5 tellurides. Conditions: background electrolyte, KCl (0.1 M); scan rate, 100 mV s^{-1}; all measurements are performed relative to the Ag/AgCl reference electrode.

Among all Group 5 TMDs, TaS_2 demonstrates fastest HET with a calculated k^0_{obs} of 3.4 × 10^{-3}cm s^{-1} that is markedly higher than the bare GC electrode. Besides this, the current intensity of the $[Fe(CN)_6]^{3-/4-}$ redox peaks generated by TaS_2 is at least 10 μA higher than the rest of the Group 5 TMDs, despite also modified with the same amount of material on the electrode. Evidently, both rapid electron transfer and higher redox current signals endow TaS_2 with properties favored in a prospective electrode material for electrochemical sensing. Corroborating with this, Zhang *et al.* has experimented with TaS_2 nanosheets as potential sensing

platforms capable of selective and sensitive detection of DNA. [57]

In contrast to TaS_2 as the best-performing Group 5 TMD in terms of HET, the Group 5 tellurides typically exhibit the slowest electron transfer rates compared to the selenides or sulfides. On average, VTe_2, $NbTe_2$ and $TaTe_2$ possess k^0_{obs} in the region of ~10^{-4} cm s^{-1} which is an order of magnitude lower than TaS_2. Moreover, the HET rates of tellurides are found to be even slower than the unmodified GC electrode. One possible explanation for the slow HET rates of tellurides is ascribed to tellurium chalcogen being most liable to surface oxidation among the chalcogenides. Significant amounts of tellurium oxides have been detected in the XPS analysis of VTe_2, $NbTe_2$ and $TaTe_2$ (Fig. S4 in ESI†), noticeably arising from TeO_2 and TeO_3. The presence of surface oxides on the tellurides may experience electrostatic repulsion from the negatively charged $[Fe(CN)_6]^{3-/4-}$ redox probes which hindered the electron transfer.

The Group 5 selenides have HET rates that are comparable to that of the GC electrode. The k^0_{obs} values of VSe_2, $NbSe_2$ and $TaSe_2$ are 1.4 × 10^{-3} cm s^{-1}, 2.7 × 10^{-3} cm s^{-1} and 1.50 × 10^{-3} cm s^{-1}, respectively, nearing that of the GC electrode.

The HET trends specific to a metal type or chalcogen type are associated with TaS_2. Considering affixing the transition metal component – tantalum, the electron transfer rate declines down the chalcogen group such that TaS_2> $TaSe_2$> $TaTe_2$. Keeping a constant chalcogen type – sulfur, improves the HET rate down the transition metal group wherein VS_2< NbS_2< TaS_2. However, these trends are not observed for an unchanged niobium and vanadium metal type or a fixed selenium and tellurium chalcogen type.

Electrocatalytic property for hydrogen evolution reaction (HER)

The electrocatalytic ability of the TMDs towards hydrogen evolution reaction (HER) has been a prime focus in the majority of electrochemical applications involving TMDs. In recent years, the promising HER performance of MoS_2 triggered a massive search within the scientific community for other layered TMDs as sustainable electrocatalysts for HER. Theoretically, metallic TMDs may outperform semiconducting TMDs as HER electrocatalysts given that computational studies affirmed the active basal planes of Group 5 TMDs, which are by nature metallic, for HER against the inert basal planes of Group 6 TMDs, which are semiconductors, including MoS_2 and WS_2.[19, 20] Fuelled by this, we investigate the HER electrocatalytic properties of Group 5 TMDs in bulk form to sieve out the best HER electrocatalyst. We also determine any metal or chalcogen dependence on their HER electrocatalytic property.

Linear sweep HER measurements have been performed for all Group 5 TMDs. Linear voltammograms are categorized according to the transition metal type in Fig. 5 and by chalcogen type in Fig. S7 (in ESI†) for an illustration of any metal- or chalcogen- dependence. As Pt/C has been recognized as the best HER electrocatalyst to date, we have included Pt/C in our experiments as a yardstick to assess the HER efficiency of the Group 5 TMDs. The polarization curve for the bare GC electrode is also shown for reference.

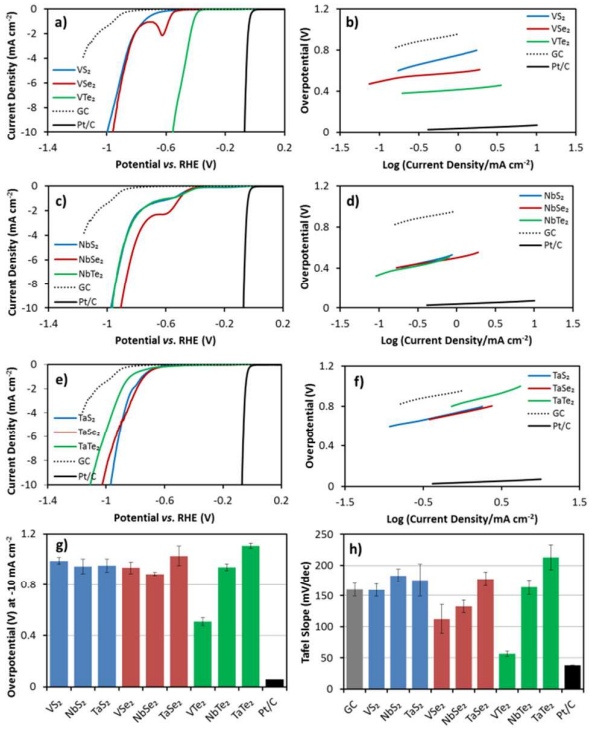

Fig. 5 Linear sweep profiles of hydrogen evolution reaction (HER) on GC electrodes modified with (a) VS_2, VSe_2 and VTe_2, (c) NbS_2, $NbSe_2$ and $NbTe_2$ and (e) TaS_2, $TaSe_2$ and $TaTe_2$. Tafel plots for HER corresponding to (b) VS_2, VSe_2 and VTe_2, (d) NbS_2, $NbSe_2$ and $NbTe_2$ and (f) TaS_2, $TaSe_2$ and $TaTe_2$. Histograms summarize the averages of (g) HER overpotential at current density of -10 mA cm^{-2} and (h) Tafel slopes for all the materials. Conditions: background electrolyte, H_2SO_4 (0.5 M); scan rate, 2 mV s^{-1}.

A reasonable gauge of the electrocatalytic performance for HER of the Group 5 TMDs is by comparing their overpotentials at a current density of -10 mA cm^{-2},[2, 4] usually corresponding to a tangible level of hydrogen production. Across all Group 5 TMDs, we observe that VTe_2 exhibits the lowest overpotential of approximately 0.5 V *vs.* RHE against most other Group 5 TMDs of overpotentials hovering in the range of 0.9 to 1.1 V *vs.* RHE. Further inspection of their overpotentials unveils a trend for the vanadium dichalcogenides such that the HER overpotentials decreases down chalcogen group, as exemplified by VS_2 at highest overpotential of 1.0 V, closely followed by VSe_2 at marginally below 1.0 V, and the lowest, VTe_2 at 0.5 V *vs.* RHE. However, such chalcogen-dependence of the HER overpotential of the Group 5 TMDs was not witnessed in niobium and tantalum dichalcogenides. All niobium dichalcogenides show comparable overpotentials whereby NbS_2, $NbSe_2$ and $NbTe_2$ differed by less than 0.1 V from each other. Analogous to the niobium dichalcogenides, the overpotentials of tantalum dichalcogenides appear to be similar as noted in little deviation of TaS_2, $TaSe_2$ and $TaTe_2$ from each other. In S7 (in ESI†), the HER overpotentials of Group 5 tellurides manifest strong transition metal-dependence with increasing overpotential in the order of VTe_2

< $NbTe_2$ < $TaTe_2$. No metal-dependence was observed for the Group 5 sulfides or selenides. Group 5 sulfides exhibit largely overlapping curves which coincide at 1.0 V *vs*. RHE at -10 mA cm^{-2}. Likewise, HER overpotentials of Group 5 selenides exist between 0.9 to 1.0 V *vs*. RHE at -10 mA cm^{-2}.

Apart from the HER overpotential at -10 mA cm^{-2}, the Tafel slope is another parameter that evaluates the electrocatalytic ability for HER and in fact, more frequently employed to elucidate the electrochemical mechanism on the TMD material. Tafel slope is understood to be the increase in overpotential required to elicit an increment in current density by one order of magnitude. By this definition, smaller Tafel slopes are preferred in a prospective HER electrocatalyst. Tafel slopes determine the rate-determining step in the HER process, providing insights into the reaction pathway undertaken by the TMD material. The main steps in the hydrogen evolution mechanism on TMD surfaces are adsorption and desorption,[3, 58] as summarized below:

1. Adsorption *via* Volmer process:
   $H_3O^+ + e \rightarrow M\text{-}H + H_2O$, $b \approx 120$ mV/dec
2. Desorption *via* Heyrovsky process:
   $M\text{-}H + H_3O^+ + e \rightarrow H_2 + H_2O + M^*$, $b \approx 40$ mV/dec
   or Desorption *via* Tafel process:
   $2\ M\text{-}H \rightarrow H_2 + 2M^*$, $b \approx 30$ mV/dec

As predicted, the Tafel slope of the most electrocatalytic Pt/C is the lowest of all with a value of 36 mV/dec and is limited by the desorption step, in accordance with reported Tafel slope values for Pt/C in the region of 30 and 40 mV/dec.[59] Out of all Group 5 TMDs, VTe_2 shows the lowest Tafel slope of 55 mV/dec. Other vanadium dichalcogenides; VS_2 and VSe_2, are respectively found to have Tafel slopes of 159 mV/dec and 112 mV/dec. Both Tafel slopes of VS_2 and VSe_2 correspond to adsorption as the slow step. Closer scrutiny of the vanadium dichalcogenides discloses that the Tafel slope lowers down the chalcogen group such that VS_2> VSe_2> VTe_2. Down the transition metal group, the Tafel slopes of Group 5 tellurides (Fig. S7, in ESI†) also increase sequentially from VTe_2 (55 mV/dec) to $NbTe_2$ (163 mV/dec) and to $TaTe_2$ with the largest Tafel value of 213 mV/dec. The niobium dichalcogenides are likely limited by the Volmer adsorption mechanism as demonstrated by Tafel slopes nearing 120 mV/dec wherein Tafel slopes of $NbSe_2$ and $NbTe_2$ are 133 mV/dec and 163 mV/dec correspondingly. There is a general observation that tantalum dichalcogenides show unusually high Tafel slope values of beyond 170 mV/dec.

We observe HER pre-waves in a few Group 5 TMDs such as VSe_2, NbS_2, $NbSe_2$ and $NbTe_2$. We draw similarities with their presence to the inherent electrochemistry discussed in the earlier section. The pre-wave occurring at *ca.* -0.7 V *vs.* RHE in VSe_2 when converted to *vs.* Ag/AgCl approximates the cathodic reduction of VSe_2 noted in Fig. 3j stemming from the surface oxides like V_2O_5. For all niobium dichalcogenides, the HER pre-wave distinctly emerges at *ca.* -0.6 V *vs.* RHE. The pre-wave resembles the shoulder signal at *ca.* -0.8 V *vs.* Ag/AgCl in the cathodic scans of NbS_2 and $NbSe_2$ due to the reduction of Nb(V) to Nb(III) species.[48, 49]

Subsequent LSV scans of VSe_2, NbS_2, $NbSe_2$ and $NbTe_2$ are recorded in Fig. S8 (ESI†) to investigate the presence of the HER pre-waves on their HER behaviour. In successive scans, these HER pre-waves disappeared or undermined in intensity. This observation parallels their inherent electrochemical profiles in Fig. 3 whereby the intrinsic reduction peaks are absent or waned in subsequent scans. The absence of HER pre-waves of VSe_2 and NbS_2 in the second scan confirms the removal of surface passivation. Unlike VSe_2 and NbS_2, HER pre-waves persist in the second scans of $NbSe_2$ and $NbTe_2$ but at a lower intensity. Apart from the role of intrinsic electrochemical reduction of $NbSe_2$ and $NbTe_2$ in engendering the HER pre-waves, another reason may boil down to the different catalytic sites coexisting on the $NbSe_2$ and $NbTe_2$. Different types of active sites on the surface contribute to varying HER activities.

Most significantly, HER pre-waves have negligible effects on the electrocatalytic efficiencies of VSe_2, NbS_2, $NbSe_2$ and $NbTe_2$ as their HER behaviour in the subsequent scans approximates the initial HER measurement (Fig. S8, in ESI†). Using second scans of VSe_2, NbS_2, $NbSe_2$ and $NbTe_2$ for comparisons (Fig. S9 and Fig. S10, in ESI†) led to identical HER trends as the initial scans. Even with the elimination of the inherent reduction peak in VSe_2, the HER efficiencies of vanadium dichalcogenides continue to show chalcogen-dependence. Furthermore, the metal-dependence of Group 5 tellurides towards their HER properties appear unaffected by the diminished HER pre-wave of $NbTe_2$ in the subsequent scan.

The presence of pre-waves may pose a challenge towards determining the onset potential for HER process for the TMDs which is usually taken at low current densities of ~-0.1 mA cm^{-2}. Pre-waves mask the onset of HER due to the dominance of the inherent electrochemical reduction in that potential window. The onset potential is unsuitable to use as a parameter to assess the HER performance under such circumstances. Therefore, to prevent a misconstrued assessment of the HER efficiency of the Group 5 TMDs arising from their inherent electrochemistry, it is essential to investigate their HER efficiency at a higher current density, as we have demonstrated here.

In view of both performance indicators by HER overpotential at -10 mA cm^{-2} and Tafel slope analyses, the highest HER electrocatalytic efficiencies within Group 5 TMDs are unanimously observed in VTe_2, clearly evident in its lowest overpotential and Tafel slope values of 0.5 V *vs.* RHE and 55 mV/dec.

The catalytic stability of the Group 5 TMDs was also studied in acidic conditions. All materials were subject to 100 cyclic voltammetry (CV) cycles in acid at their respective HER onset potential window where the current density reached is at least -0.1 mA cm^{-1}. The HER polarisation curves before and after the 100 CVs are recorded in Fig. S11 (ESI†). It is broadly noted that all Group 5 TMDs are relatively stable in acid with no more than 0.1 V deviation between their HER overpotentials at -10 mA cm^{-2} before and after 100 CVs. While a mildly deteriorated HER performance was noted for Group 5 sulfides and tellurides, the Group 5 selenides show slightly improved HER behaviour requiring lower overpotentials. During the CV cycles

in acidic medium, adsorbed species are likely removed or the active sites may become chemically changed. These factors contribute to the minor differences in HER behaviour after performing CV cycles in acid. To a large extent, the Group 5 TMDs demonstrate robust catalytic stability in acid with minimal shifts in their HER overpotentials at -10 mA cm^{-2}.

Density functional theory (DFT) calculations

We calculate the differential adsorption enthalpies of hydrogen to tantalum and niobium dichalcogenides. According to calculated results, the basal planes could become active at higher overpotential, because their adsorption enthalpies approach that of thermoneutral. The basal plane of TaS_2 and $TaSe_2$ has ΔG_H of 0.24 eV and 0.61 eV, respectively. This is in striking contrast to MoS_2, in which the hydrogen adsorption onto basal plane is highly endothermic and the active sites for HER were experimentally determined to be at the edges rather than at the basal planes.[14] Nevertheless, the edge sites provide more favourable adsorption enthalpies than their basal planes for both TaS_2 and $TaSe_2$. TaS_2 has ΔG_H of -0.09 eV at 50 % hydrogen coverage, while $TaSe_2$ has ΔG_H of 0.01 eV at 25 % hydrogen coverage. Our ΔG_H values and optimal coverage agree well to recent DFT study by Tsai *et al.*[20] Both ΔG_H values lie close to zero, which is an ideal value according to the Sabatier's principle. Niobium dichalcogenides show an adsorption character very similar to their tantalum counterparts. Fig. 6 reveals that the hydrogen atom adheres more strongly to the edge of Ta and Nb disulfide than diselenide over the whole coverage range, while the chemical nature of the metal atom seems to be of minor influence. The trend of the increasing adsorption enthalpy as one descends through the group of dichalcogenides has been recently observed for platinum dichalcogenides.[60] The explanation of the trend lies mainly in the size of chalcogenide atom. As the size of chalcogenide atom increases, the bonding orbitals become larger and more diffused and, consequently, the bond between the atom and the hydrogen weakens. Fig. 6 also shows that ΔG_H strongly increases at high hydrogen coverage, because adsorbed hydrogens repel each other.

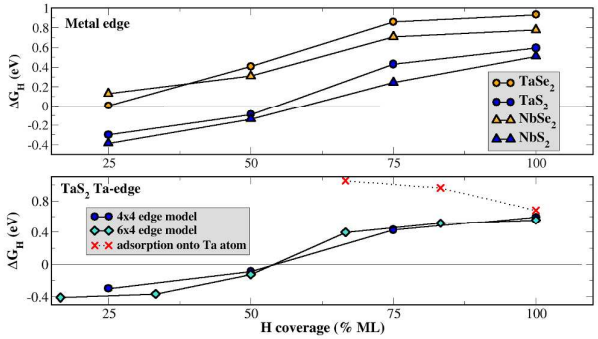

Fig. 6 The differential adsorption enthalpy ΔG_H of hydrogen to the edge of 2H-TaS_2, $TaSe_2$, NbS_2 and $NbSe_2$ calculated as a function of the edge coverage (upper panel). Lower panel shows ΔG_H of TaS_2 calculated on two edge models (nanostripe four and six units long). Crosses show ΔG_H for the hydrogen adsorption directly onto the Ta atom at the edge.

Therefore, both previous computational screening[20] and our calculations suggest based on favourable ΔG_H that both TaS_2 and $TaSe_2$ shall be good HER catalysts, whereas our experimental results show only modest performance of them. This discord indicates there are other critical factors toward HER performance than ΔG_H only. Indeed, recent study by Huang *et al.*[61] of reaction mechanism of HER on MoS_2 found that ΔG_H did not play a direct role in determining the reaction barrier. Huang *et al.* revealed that the Volmer-Tafel reaction took place between hydrogens on adjacent Mo and S atoms. The hydrogen was adsorbed on the sulphur first as suggested by favourable ΔG_H, but then migrated to the molybdenum atom and finally reacted with a proton to form H_2. The hydrogen adsorbed at the Mo atom was therefore an important intermediate in the process. In this spirit, we calculate ΔG_H for hydrogen adsorption on the Ta atom at edge. The Ta-H intermediate seems however to be unlikely, because respective ΔG_H values are highly positive (Fig. 6). The lowest ΔG_H of 0.68 eV is obtained for the 100 % coverage, but even at that coverage the adsorption onto sulphur atom is more favourable. Therefore, too high energy of the Ta-H intermediate may force hydrogen evolution to proceed via less effective mechanism and limit overall HER performance of tantalum dichalcogenides.

Nevertheless, there are further factors that may influence the HER efficiency of TMDs, such as the conductivity of the TMD, and number of active sites. In order to inspect the latter factor, we calculate ΔG_H using a larger edge model, which comprises six Ta atoms along the edge and offers a broader range of hydrogen coverage (Fig. 6, lower panel). Although ΔG_H values are essentially close to those calculated for four atoms long edge, it becomes clear that the ΔG_H is close to thermoneutral for a narrow range around 50 % coverage only. A narrow range of effective hydrogen coverage may kinetically hamper HER performance of the TaS_2. Furthermore, experimental results allude that the method of synthesis and number of the layers of the TMDs could have elicited electrocatalytic behaviour different than that expected from theory. Our as-synthesized bulk VS_2 exhibits large Tafel slope of 159 mV/dec and overpotential at 0.9 V *vs.* RHE which is strikingly dissimilar to the chemically vapor deposited VS_2.[21] Yuan *et al.* reported that VS_2 nanosheets synthesized by chemical vapor deposition displayed impressive HER performance as manifested in its Tafel slope of 34 mV/dec rivalling that of Pt and a low HER overpotential of 68 mV *vs.* RHE at a current density of -10 mA cm^{-2}.[21]

Despite theoretical indications that the metallic Group 5 TMDs could outshine the semiconducting Group 6 TMDs as efficient electrocatalysts for HER, it has been experimentally shown to be otherwise. Among measured Group 5 dichalcogenides, only VTe_2 appears to be promising as the HER electrocatalyst. However, it is crucial to highlight that theoretical calculations consider firstly an idealized edge model – the ideal clean straight edge of single layered TMDs,

and secondly only thermodynamics, the hydrogen adsorption enthalpy, while it is reaction barrier that determines the rate. Our experimental results thus provide a challenge for the future, more detailed, theoretical studies.

Experimental

Materials

Potassium ferrocyanide, hexaammineruthenium (III) chloride, potassium chloride, potassium phosphate dibasic, sodium phosphate monobasic, sodium chloride, sulfuric acid and platinum on carbon were purchased from Sigma Aldrich. Pt, Ag/AgCl and glassy carbon (GC) electrodes were purchased from CH Instruments, Texas, USA. The bulk Group 5 transition metal dichalcogenides: VS_2, VSe_2, VTe_2, NbS_2, $NbSe_2$, $NbTe_2$, TaS_2, $TaSe_2$ and $TaTe_2$ were obtained from Aldrich.

Apparatus

X-ray photoelectron spectroscopy (XPS) was performed with a Phoibos 100 spectrometer with a monochromatic Mg K_α radiation as the X-ray source (SPECS, Germany). Survey scans were generated for all the nine samples. High-resolution spectra were also obtained for the Group 5 metals: V 2p, Nb 3d and Ta 4f; and their corresponding chalcogens: S 2p, Se 3d and Te 3d. The signals were calibrated using adventitious carbon at 284.5 eV. We considered relative sensitivity factors during the calculation of chalcogen-to-metal ratios and the deconvolution of V 2p, Nb 3d and Ta 4f. The deconvolution of V 2p, Nb 3d and Ta 4f was based on various oxidation states, using the oxides as a basis. Best curve fits for the high-resolution XPS spectra of V 2p, Nb 3d and Ta 4f were performed using the ratio of V $2p_{3/2}$ and V $2p_{1/2}$ doublet signals as 2:1; Nb $3d_{5/2}$ and Nb $3d_{3/2}$ as 3:2; and Ta $4f_{7/2}$ and Ta $4f_{5/2}$ as 4:3.

Scanning electron microscopy (SEM) was conducted on a JEOL 7600F field-emission scanning electron microscope (JEOL, Japan) either at gentle-beam mode at 2.0 kV or SEM mode at 50 kV. Energy dispersive X-ray spectroscopy (EDS) data was obtained using an accelerating voltage of 20.0 kV.

Voltammetric measurements were recorded on a μAutolab III electrochemical analyser (Eco Chemie B.V., Utrecht, The Netherlands) with the software NOVA version 1.8 (Eco Chemie). Electrochemical measurements of the transition metal dichalcogenide (TMD) materials were performed in a 3 mL voltammetric cell at room temperature (25 ^{0}C) in a default three electrode configuration. A platinum electrode and an Ag/AgCl electrode (1 M KCl) functioned as auxiliary and reference electrodes, respectively and a glassy carbon (GC, 3 mm diameter) electrode was adopted as the working electrode.

Procedures

Fundamental electrochemical studies were performed in 50 mM phosphate buffered saline (PBS) as the background electrolyte at pH 7. All cyclic voltammetry experiments were conducted at a scan rate of 100 mV s^{-1}. The voltammetric scan began at 0 V *vs.* Ag/AgCl; the potential at which redox processes were not expected to occur,[62] and scanned towards 1.8 V followed by a reverse sweep to -1.8 V for the anodic study and first towards -1.8 V followed by a reverse sweep to 1.8 V for the cathodic study before returning to 0 V. The nine TMD materials: VS_2, VSe_2, VTe_2, NbS_2, $NbSe_2$, $NbTe_2$, TaS_2, $TaSe_2$ and $TaTe_2$ samples were prepared in concentrations of 1 mg mL^{-1} in deionised water and subject to first-time ultrasonication for 2.5 h to attain well-dispersed suspensions. Prior to each electrochemical measurement, the samples were ultrasonicated for a period of 20 minutes to maintain the homogeneous dispersion of the desired material. 4.0 μL aliquot of the suspension was then drop casted on a GC electrode and dried to yield an electrode surface modified with 4.0 μg film of the desired material.

Studies on heterogeneous electron transfer (HET) at TMD surfaces were executed in potassium chloride (0.1 M) as the supporting electrolyte for potassium ferrocyanide (5 mM) redox probe. Cyclic voltammetry scans were performed at a rate of 100 mV s^{-1}. To eliminate interference due to inherent electrochemistry, the first scan has been excluded. Instead, data from subsequent scans are used. The k^0_{obs} values were calculated using the method devised by Nicholson that relates ΔE_p to a dimensionless parameter Ψ and consequently into $k^0_{obs.}$[63] The roughness of the electrode was not considered in the calculation of $k^0_{obs.}$ The diffusion coefficient D = 7.26×10^{-6} cm^2 s^{-1} was used to compute k^0_{obs} values for $[Fe(CN)_6]^{4-/3-}$.[64]

Hydrogen evolution reaction (HER) measurements of these TMD materials were carried out using linear sweep voltammetry at a scan rate of 2 mV s^{-1} in 0.5 M H_2SO_4 electrolyte. Linear sweep voltammograms are presented *versus* the reversible hydrogen electrode (RHE) using and the measured potentials are calculated using this equation[65] $E_{RHE} = E_{Ag/AgCl} + 0.059 \times pH + E^0_{Ag/AgCl}$ where $E_{Ag/AgCl}$ is the measured potential, pH of 0.5 M H_2SO_4 electrolyte is zero and $E^0_{Ag/AgCl}$ refers to the standard potential of Ag/AgCl (1 M KCl) at 25 °C which is 0.235 V. Current density (mA cm^{-2}) was calculated using the geometric area of the GC electrode (0.07 cm^2). The exchange current density (*j*) provided in Table S7 (ESI†) was determined from the respective Tafel regions of the TMD materials where the overpotential is 0 V *vs.* RHE.

The HER catalytic stability of the all TMDs were performed in 0.5 M H_2SO_4 electrolyte before and after 100 cyclic voltammetric scans at 100 mV s^{-1}. The cyclic voltammetric scan range of each of the Group 5 TMD corresponds to their HER onset region where the current density is at least -0.1 mA cm^{-2}. For VS_2, VSe_2, VTe_2, NbS_2 and $NbSe_2$ materials, the cyclic voltammetric scan range is conducted from -0.235 V to -0.635 V *vs.* Ag/AgCl. The scan window is from -0.435 to -0.835 V and -0.535 to -0.935 V *vs.* Ag/AgCl for respectively TaS_2 and $NbTe_2$. $TaSe_2$ and $TaTe_2$ are scanned from -0.335 to -0.735 V *vs.* Ag/AgCl.

Theoretical methods

DFT calculations were performed using the projector-augmented wave method implemented in the Vienna Ab initio Simulation Package (VASP). [66, 67] Bond covalency analysis was also performed.[68] The energy cutoff for the plane-wave expansion was set to 350 eV. We used optimized van der Waals functional optB86b-vdW functional,[69] which described very well the structural properties of various TaS_2 phases according to recent study.[70] We calculated the catalytic properties of TaS_2, $TaSe_2$, and $NbSe_2$, because they possess the same 2H crystal structure which separates the influence of the structure and chemical composition. For comparison, we also included the 2H-NbS_2. The free energy of the adsorption of atomic hydrogen (ΔG_H) is a quantity which can be used to describe the HER activity of the catalyst.[14] The ΔG_H of an ideal catalyst for HER should be as close to 0 as possible. We considered the adsorption of hydrogen onto the surface and edge sites of single layered dichalcogenides. The surface (basal plane) was modeled by a 4×4 supercell (16 Ta or Nb atoms) in connection with 3×3×1 k-point sampling. The layers were separated by 18 Å of vacuum. The edge was modeled by a 4×4 nanostripe, i.e. it contained four atoms along the edge and the nanostripe was four atoms wide. The nanostripe model of the as-cleaved edge of the 2H structure exposed both chalcogen terminated edge and metal terminated edge. Their specific structure (the coverage of chalcogen atoms on the edge) mainly depends on the chemical potential of sulphur containing compounds under the operating conditions. We focused on the metal terminated edge. We found that the most stable coverage for TaS_2 is at 50 % chalcogen coverage, which is in accordance with earlier detailed study for MoS_2.[71] We therefore used 50 % coverage of the edge for all four dichalcogenides. The Brillouin zone of the nanostripe was sampled by 1×3×1 k-points where three k-points belonged to the only direction in which the cell was periodically repeated. As the edge contained four adsorption sites on sulphur and selenium atoms, possible hydrogen coverages of the edge were 25%, 50%, 75%, and 100%. The edge was gradually (one-by-one) covered with hydrogen atoms and the differential energy of adsorption ΔE was calculated as $\Delta E = E_{TOT}(nH^*) - E_{TOT}[(n\text{-}1)H^*] - 1/2\ E_{TOT}(H_2)$. The Gibbs free-energy of the adsorption atomic hydrogen (ΔG_H) was obtained as $\Delta G_H = \Delta E + \Delta E_{ZPE} - T\Delta S_H$, where ΔE_{ZPE} and ΔS_H was the difference in zero point energy, and entropy between the adsorbed hydrogen and hydrogen in the gas phase. These thermal corrections were found to be independent of particular adsorption site, and thus ΔG_H at standard condition was determined by ΔE plus a thermal correction constant of 0.29 eV.[14]

Conclusions

In closing, we have elucidated the inherent electrochemistry, and explored the electrochemical property of heterogeneous electron transfer (HET) and the electrocatalytic performance for hydrogen evolution reaction (HER) of the nine Group 5 TMDs in the bulk form; namely, VS_2, VSe_2, VTe_2, NbS_2, $NbSe_2$, $NbTe_2$, TaS_2, $TaSe_2$ and $TaTe_2$. Their surface morphology, elemental and surface composition also have been systematically examined by SEM-EDX and XPS. The inherent electrochemistry of Group 5 TMDs has been ascribed to the electrochemical processes intrinsic to their constituent metal or chalcogen and the presence of surface oxides when potentials are applied. Moreover, among all Group 5 TMDs, we have shown that TaS_2 possesses fastest heterogeneous electron transfer (HET) rate at 3.4×10^{-3} cm s^{-1} which renders TaS_2 a suitable electrode material for electrochemical sensing applications. Compared to sulfides and selenides, slower HET rates have been consistently observed in the tellurides with magnitude of ~10^{-4} cm s^{-1}. In the aspect of HER performance, VTe_2 has been identified as the best electrocatalyst for HER in terms of HER overpotential and Tafel slope, at 0.5 V *vs.* RHE and 55 mV/dec, respectively. While VTe_2 demonstrates impressive HER performance, other Group 5 TMDs generally show average HER performance, falling short of initial expectations. Within the vanadium dichalcogenides, the HER performance is correlated to the chalcogen type; whereby the electrocatalytic property increases down the chalcogen group such that $VS_2 < VSe_2 < VTe_2$. Additionally, the Group 5 tellurides exhibit transition-metal dependence whereby the HER performance adheres to the trend of $VTe_2 > NbTe_2 > TaTe_2$. Density functional theory (DFT) calculations for niobium and tantalum dichalcogenides have been executed. With the aid of our theoretical studies, we have also addressed the HER performance of Group 5 TMDs on the premises of thermodynamics and kinetics. Hence, this fundamental study on Group 5 TMDs has shed light on their electrochemical and electrocatalytic attributes. It is worthwhile to highlight that TaS_2 has distinctly fast HET rates that may be potentially exploited in sensing devices while the remarkable HER performance of VTe_2 deems it a competitive earth-abundant electrocatalyst for hydrogen evolution.

Acknowledgements

M.P. acknowledges funding from Ministry of Education (Singapore) from Tier RGT1/13. P.L. acknowledges the support by the LO1305 of the Ministry of Education, Youth and Sports of Czech Republic. Z.S was supported by Czech Sience Foundation (GACR No. 15-07912S and GACR No. 16-05167S) and Specific University Research (MSMT No. 20/2015).

Notes and references

1 F. Wang, J. Li, F. Wang, T. A. Shifa, Z. Cheng, Z. Wang, K. Xu, X. Zhan, Q. Wang, Y. Huang, C. Jiang, J. He, *Adv. Funct. Mater.* 2015**, 25**, 6077-6083.
2 X. Chia, A. Ambrosi, Z. Sofer, J. Luxa, M. Pumera, *ACS Nano* 2015**, 9**, 5164-5179.
3 Y. Li, H. Wang, L. Xie, Y. Liang, G. Hong, H. Dai, *J. Am. Chem. Soc.* 2011, **133**, 7296-7299.

4 J. D. Benck, T. R. Hellstern, J. Kibsgaard, P. Chakthranont, T.F. Jaramillo, *ACS Catal.* 2014, **4**, 3957-3971.
5 G. Ye, Y. Gong, J. Lin, B. Li, Y. He, S. T. Pantelides, W. Zhou, R. Vajtai, P. M. Ajayan, *Nano Lett.* 2016, **16**, 1097-1103.
6 J. Zhou, *Appl. Mater. Today* 2016, **2**, 24-56.
7 S. Wu, Z. Zeng, Q. He, Z. Wang, S.J. Wang, Y. Du, Z. Yin, X. Sun, W. Chen, H. Zhang, *Small* 2012, **8**, 2264-2270.
8 M. Acerce, D. Voiry, M. Chhowalla, *Nat Nanotechnol.* 2015, **10**, 313-318.
9 T. Stephenson, Z. Li, B. Olsen, D. Mitlin, *Energy Environ. Sci.* 2014, **7**, 209-231.
10 Z. He, W. Que, *Appl. Mater. Today* 2016, **3**, 23-56.
11 J. A. Wilson, F. J. Di Salvo, S. Mahajan, *Phys. Rev. Lett.* 1974, **32**, 882-885.
12 B. Sipos, A. F. Kusmartseva, A. Akrap, H. Berger, L. Forro, E. Tutis, *Nat. Mater.* 2008, **7**, 960-965.
13 M. S. Dresselhaus, I. L. Thomas, *Nature* 2001, **414**, 332-337.
14 B. Hinnemann, P. G. Moses, J. Bonde, K. P. Jørgensen, J. H. Nielsen, S. Horch, I. Chorkendorff, J. K. Nørskov, *J. Am. Chem. Soc.* 2005, **127**, 5308-5309.
15 T. F. Jaramillo, K. P. Jørgensen, J. Bonde, J. H. Nielsen, S. Horch, I. Chorkendorff, *Science* 2007, **317**, 100-102.
16 C. Tsai, K. Chan, F. Abild-Pedersen, J. K. Norskov, *Phys. Chem. Chem. Phys.* 2014, **16**, 13156-13164.
17 J. R. McKone, A. P. Pieterick, H. B. Gray, N. S. Lewis, *J. Am. Chem. Soc.* 2013, **135**, 223-231.
18 D. Voiry, H. Yamaguchi, J. Li, R. Silva, D. C. B. Alves, T. Fujita, M. Chen, T. Asefa, V. B. Shenoy, V. G. Eda, M. Chhowalla, *Nat. Mater.* 2013, **12**, 850-855.
19 H. Pan, *Sci. Rep.* 2014, **4**, 5348.
20 C. Tsai, K. Chan, J. K. Nørskov, F. Abild-Pedersen, *Surf. Sci.* 2015, **640**, 133-140.
21 J. Yuan, J. Wu, W. J. Hardy, P. Loya, M. Lou, Y. Yang, S. Najmaei, M. Jiang, F. Qin, K. Keyshar, H. Ji, W. Gao, J. Bao, J. Kono, D. Natelson, P. M. Ajayan, J. Lou, *Adv. Mater.* 2015, **27**, 5605-5609.
22 M. Chhowalla, H. S. Shin, G. Eda, L.-J. Li, K. P. Loh, H. Zhang, *Nat. Chem.* 2013, **5**, 263-275.
23 M. A. Lukowski, A. S. Daniel, F. Meng, A. Forticaux, L. Li, S. Jin, *J. Am. Chem. Soc.* 2013, **135**, 10274-10277.
24 G. Silversmit, D. Depla, H. Poelman, G. B. Marin, R. De Gryse, *J. Electron Spectrosc. Relat. Phenom.* 2004, **135**, 167-175.
25 C. S. Rout, B.-H. Kim, X. Xu, J. Yang, H. Y. Jeong, D. Odkhuu, N. Park, J. Cho, H. S. Shin, *J. Am. Chem. Soc.* 2013, **135**, 8720-8725.
26 G. E. McGuire, G. K. Schweitzer, T. A. Carlson, *Inorg. Chem.* 1973, **12**, 2450-2453.
27 M. K. Bahl, *J. Phys. Chem. Solids* 1975, **36**, 485-491.
28 F. J. Berry, M. E. Brett, R. A. Marbrow, W. R. Patterson, *J. Chem. Soc., Dalton Trans.* 1984, **985-987**.
29 M. Demeter, M. Neumann, W. Reichelt, *Surf. Sci.* 2000, **454–456**, 41-44.
30 A. F. Holleman, E. Wiberg, *Inorganic Chemistry*. Walter de Gruyter GmbH & Co.: Berlin, 2001.
31 Q. Ma, R. A. Rosenberg, *Appl. Surf. Sci.* 2003, **206**, 209-217.
32 S. Lecuyer, A. Quemerais, G. Jezequel, *Surf. Interface Anal.* **1992,** *18*, 257-261.
33 A. Ispas, B. Adolphi, A. Bund, F. Endres, *Phys. Chem. Chem. Phys.* 2010, **12**, 1793-1803.
34 A. A. Audi, P. M. A. Sherwood, *Surf. Interface Anal.* 2000, **29**, 265-275.
35 M. Shenasa, S. Sainkar, D. Lichtman, *J. Electron Spectrosc. Relat. Phenom.* 1986, **40**, 329-337.
36 F. Garbassi, J. C. J. Bart, G. Petrini, *J. Electron Spectrosc. Relat. Phenom.* 1981, **22**, 95-107.
37 L. V. Yashina, S. P. Kobeleva, T. B. Shatalova, V. P. Zlomanov, V. I. Shtanov, *Solid State Ionics* 2001, **141–142**, 513-522.
38 Y. A. Teterin, V. I. Nefedov, M. F. Churbanov, A. Y. Teterin, K. I. Maslakov, E. V. Zorin, *Inorg. Chem.* 2007, **43**, 888-896.
39 W. Jaegermann, D. Schmeisser, *Surf. Sci.* 1986, **165**, 143-160.
40 X. Chia, A. Y. S. Eng, A. Ambrosi, S. M. Tan, M. Pumera, *Chem. Rev.* 2015, **115**, 11941-11966.
41 M. Z. M. Nasir, Z. Sofer, A. Ambrosi, M. Pumera, *Nanoscale* 2015, **7**, 3126-3129.
42 D. M. Ryan, T. L. Riechel, T. Welton, *J. Electrochem. Soc.* 2002, **149**, A371-A378.
43 G. W. Mellors, S. Senderoff, *J. Electrochem. Soc.* 1965, **112**, 266-272.
44 M. Pourbaix, *Atlas of Electrochemical Equilibria in Aqueous Solutions*. National Association of Corrosion Engineers: Michigan, 1974.
45 S. Sapra, H. Li, Z. Wang, I. I. Suni, *J. Electrochem. Soc.* 2005, **152**, B193-B197.
46 F. Lantelme, Y. Berghoute, *J. Electrochem. Soc.* 1994, **141**, 3306-3311.
47 S. B. Basame, H. S. White, *Langmuir* 1999, **15**, 819-825.
48 S. Zeltzer, *Collect. Czech. Chem. Commun.* 1932, **4**, 319-334.
49 L. R. Sherman, V. S. Archer, *Anal. Chem.* 1970, **42**, 1356-1361.
50 V. Venkatasamy, N. Jayaraju, S. M. Cox, C. Thambidurai, M. Mathe, J. L. Stickney, *J. Electroanal. Chem.* 2006, **589**, 195-202.
51 C. Tsang, Y.-G. Kim, D. Gebregziabiher, J. Stickney, *J. Electrochem. Soc.* 2013, **160**, D3278-D3284.
52 D. Brookins, Tellurium in *Eh-pH Diagrams for Geochemistry*, Springer-Verlag, Berlin Heidelberg, 1988, 20-21.
53 D. Brookins, Selenium in *Eh-pH Diagrams for Geochemistry*, Springer-Verlag, Berlin Heidelberg, 1988, 18-19.
54 D. Brookins, Sulphur in *Eh-pH Diagrams for Geochemistry*, Springer-Verlag, Berlin Heidelberg, 1988, 16-17.
55 J. J. Lingane, L. W. Niedrach, *J. Am. Chem. Soc.* 1948, **70**, 4115-4120.
56 R. L. McCreery, *Chem. Rev.* 2008, **108**, 2646-2687.
57 Y. Zhang, B. Zheng, C. Zhu, X. Zhang, C. Tan, H. Li, B. Chen, J. Yang, J. Chen, Y. Huang, L. Wang, H. Zhang, *Adv. Mater.* 2015, **27**, 935-939.
58 J. G. N. Thomas, *Trans. Faraday Soc.* 1961, **57**, 1603-1611.
59 B. E. Conway, B. V. Tilak, *Electrochim. Acta* 2002, **47**, 3571-3594.
60 X. Chia, A. Ambrosi, P. Lazar, Z. Sofer, J. Luxa, M. Pumera, *Adv. Funct. Mater.* 2016, **26**, 4306-4318.
61 Y. F. Huang, R. J. Nielsen, W. A. Goddard, M. P. Soriaga, *J. Am. Chem. Soc.* 2015, **137**, 6692-6698.
62 R. G. Compton, C. E. Banks, *Understanding Voltammetry*. World Scientific Publishing Co. Pte. Ltd., Singapore, 2007.
63 R. S. Nicholson, *Anal. Chem.* 1965, **37**, 1351-1355.
64 S. J. Konopka, B. McDuffie, *Anal. Chem.* 1970, **42**, 1741-1746.
65 S. Hoang, S. Guo, N. T. Hahn, A. J. Bard, C. B. Mullins, *Nano. Lett.* 2012, **12**, 26-32.
66 P. E. Blochl, *Phys. Rev. B* 1994, **50**, 17953.
67 G. Kresse, D. Joubert, *Phys. Rev. B* 1999, **59**, 1758.
68 A. Cammarata, J. M. Rondinelli, *J. Chem. Phys.* 2014, **141**, 114704.
69 J. Klimes, D. R. Bowler, A. Michaelides, *Phys. Rev. B* 2011, **83**, 195131.
70 P. Lazar, J. Martincova, M. Otyepka, *Phys. Rev. B* 2015, **92**, 224104.
71 P. Raybaud, J. Hafner, G. Kresse, S. Kasztelan, H. Toulhoat, *J. Catal.* 2000, **189**, 129-146.

Manuscript ID: TA-ART-06-2016-005110

Title: Electrocatalysis of layered Group 5 metallic transition metal dichalcogenides (MX_2, M=V, Nb, Ta; X= S, Se, Te)

Authors: *Xinyi Chia, Adriano Ambrosi, Petr Lazar, Zdeněk Sofer and Martin Pumera**

Journal: Journal of Materials Chemistry A

Table of Contents (ToC)

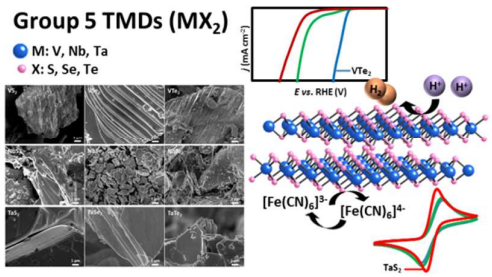

Here, we unravel trends of layered Group 5 transition metal dichalcogenides in aspects of their electrocatalytic hydrogen evolution and electrochemistry.